infection, any unintegrated DNA forms were not detected and all of HIV-1-specific DNA was randomly integrated in the MT-4/CS-CG cells (Fig. 2C, lane 6). Then, we measured individual forms of viral DNA in the cells by real-time PCR with specific primers and probes (Fig. 1). The average copy number of R/U5 and U5/gag DNA was consistently $7,474 \pm 715$ in 100 ng of the MT4/CS-CG DNA, and the amount of 2-LTR circle was below the detection level (data not shown), consisting with the result of Southern blot analysis (Fig. 2C, lane 6). Because the HIV-1 vector, CS-CG is replication-incompetent, these results indicate that the detected DNA was integrated form in this cell line.

Development of Quantitative Alu-*HIV PCR Assay by Real-time PCR*

We next attempted to detect the randomly integrated DNA in MT4/CS-CG cells by *Alu*-HIV with real-time PCR. A set of serially diluted total DNA samples (0.1, 0.5, 1, 5, 10, 50, and 100 ng) from the MT4/CS-CG cells was subjected to first round of PCR using the primers for *Alu* and HIV-1 sequences (Fig. 1). Subsequently, the first PCR product was diluted 100-, 1,000-, and 10,000-fold and subjected to real-time PCR using primers to detect R/U5 DNA (Fig. 1). As a negative control, the same amount of DNA from MT4/CS-CG was subjected to first round of PCR in the absence of DNA polymerase. As shown in Fig. 3 (top panels), an inverse linear curve was obtained by plotting the amount of input DNA in the first round of PCR against the number of the threshold cycle (C_T) in the subsequent real-time PCR assay for R/U5 DNA. Thus, a standard curve was obtained using DNA from the MT4/CS-CG cells, in which the copy number of viral DNA is known, that could be used to measure the integrated DNA in samples. Although the negative control yielded low numbers of C_T in the 100- and 1,000-fold diluted samples, when more than 10 ng DNA was used in the first round of PCR, these background were not observed in further diluted samples (10,000-fold) of the negative control (Fig. 3, top panels, right). These results demonstrated that by performing multiple dilutions of the samples after the first round of PCR we could eliminate the background. Thus, we established an assay for measuring varying amounts of the integrated DNA. The reliable range of this assay was from as low as 7 copies per reaction. An inverse linear curve was also obtained by plotting the amount of input DNA from another infected cells, ACH2, in the first round of PCR against the number of C_T in the subsequent real-time PCR assay (Fig. 3, bottom panels). This cell line is latently infected with HIV-1 and the most viral DNA is known as the integrated form [27]. Therefore, we conclude that our PCR assay is highly quantitative and applicable to the measurement of the integrated DNA.

Application of the Real-time PCR Assay for Early Phase of Infection

We further evaluated our real-time PCR assay by comparing the each viral DNA forms of luciferase-expressing HIV-1 with site-directed or deletion mutations in the integrase (D116G [21]), Vpr (ΔVpr [15]), or PBS (ΔPBS) genes. Because in this experiment, we used VSV-G-pseudotyped HIV-1, it was possible to introduce large amounts of viral RNA into target cells [21,22]. Thus, we could detect a sufficient amount of viral DNA in infected cells to estimate the precise efficiency of reverse transcription and integration in a single round of infection. The copy number of strong-stop DNA was calculated by subtracting the number of U5/gag DNA copies from the number of R/U5 DNA copies. The copy number of the unintegrated full-length DNA and 1-LTR circles (full-length/1-LTR) was calculated by subtracting the number of 2-LTR DNA and integrated DNA copies from the number of U5/gag DNA copies (Fig. 1). The VSV-G-pseudotyped WT and mutant viruses were generated by co-transfection into 293T cells. There was no apparent difference in the level of $p24^{gag}$ in the culture supernatant and the level of luciferase activity in the lysate from transfected cells (Fig. 4A), confirming that none of the mutations had a significant effect on the level of viral gene expression and virus release [15,21]. In ΔVpr-infected cells the level of 2-LTR circle and integrated DNA were similar to those in WT-infected cells (Fig. 4A, WT and ΔVpr). In contrast, severe impairment of the integration and markedly increased levels of all unintegrated DNA forms (strong-stop, full-length/1-LTR, and 2-LTR circle) were found in D116G-infected cells (Fig. 4A, D116G). In ΔPBS-infected cells, significant impairment of the initiation of reverse transcription was observed (Fig. 4A,

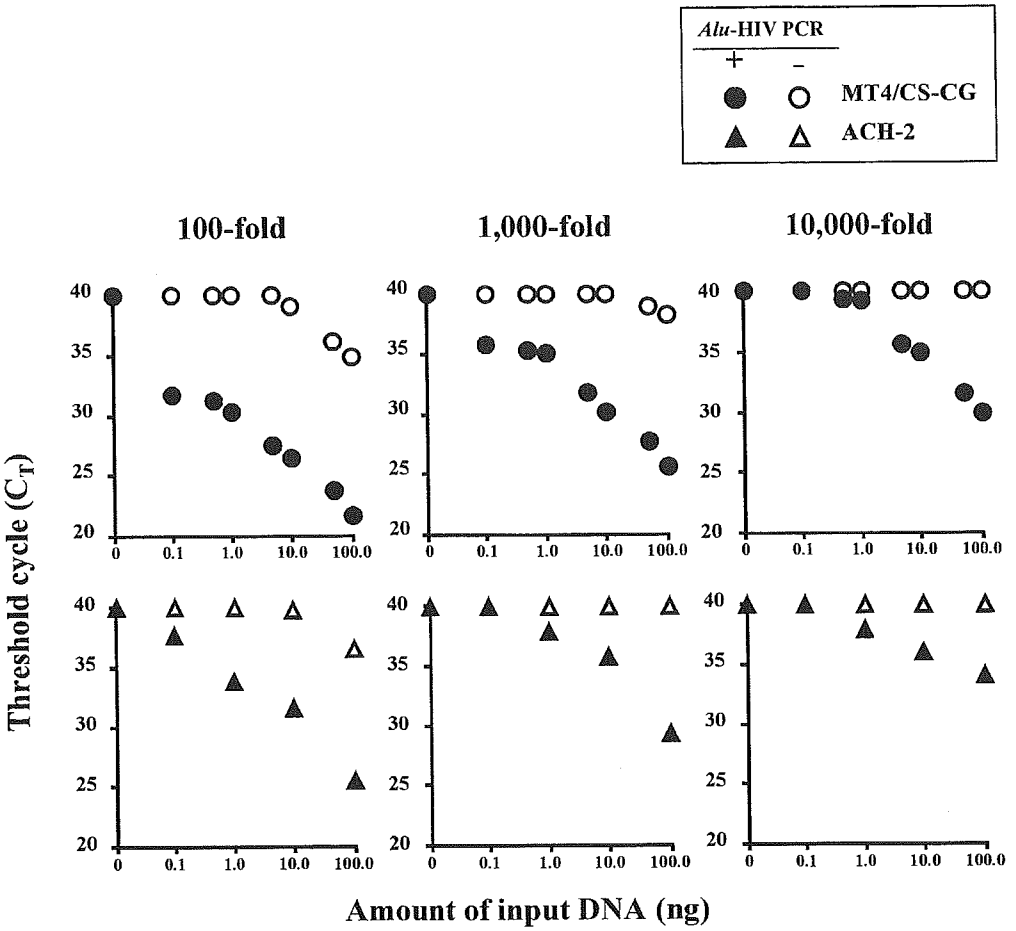

Fig. 3. Standard curves for the amount of integrated DNA amplified by PCR. The total DNA was extracted from MT4/CS-CG (top panels) and ACH-2 (bottom panels) cells and 0.1–100 ng genomic DNA was amplified in the first round of PCR using *Alu*- and HIV-1-specific primers. As a negative control, the same amount of DNA was subjected to the first round of PCR without DNA polymerase. Next, the products from the first round of PCR (closed symbols) and the negative control (open symbols) were diluted 100-, 1,000-, or 10,000-fold and subjected to real-time PCR using sense primer M667, antisense primer AA55, and fluorogenic probe HIV-FAM. The threshold cycle obtained in the real-time PCR (C_T) was plotted against the amount of input DNA subjected to the first round of PCR. The data are from three independent experiments and all SD are below 1.0 (data not shown).

ΔPBS) [28]. Finally, luciferase activity in ΔVpr-infected cells was slightly higher than in WT-infected cells (Fig. 4B, 676,112 ± 61,625 versus 505,682 ± 78,451 relative light units/μg protein), whereas the level of integrated DNA in ΔVpr-infected cells was slightly lower than in WT-infected cells (Fig. 4A, 8,583.5 ± 537.7 versus 9,622 ± 142.8 copies). We also examined the kinetics of each form of HIV-1 DNA. Synthesis of strong-stop DNA was almost complete by 4 h after infection (data not shown). As seen in Southern blot analysis the full-length, 2-LTR circle, and integrated forms of viral DNA gradually increased at later time points after infection (data not shown). Therefore, these data confirmed that our PCR assay is reliable and useful to evaluate the events occurring in the early steps of HIV-1 infection.

Integration Efficiency of HIV-1 in Stimulated and Unstimulated PBMC Culture

Some studies have demonstrated that freshly isolated PBMC are resistant to the establishment of productive infection by HIV-1 and simian immunodeficiency virus (SIV) [17,29,30]. Although it is well known that the impairments of reverse transcription step are observed [8,10,17], the efficiency of

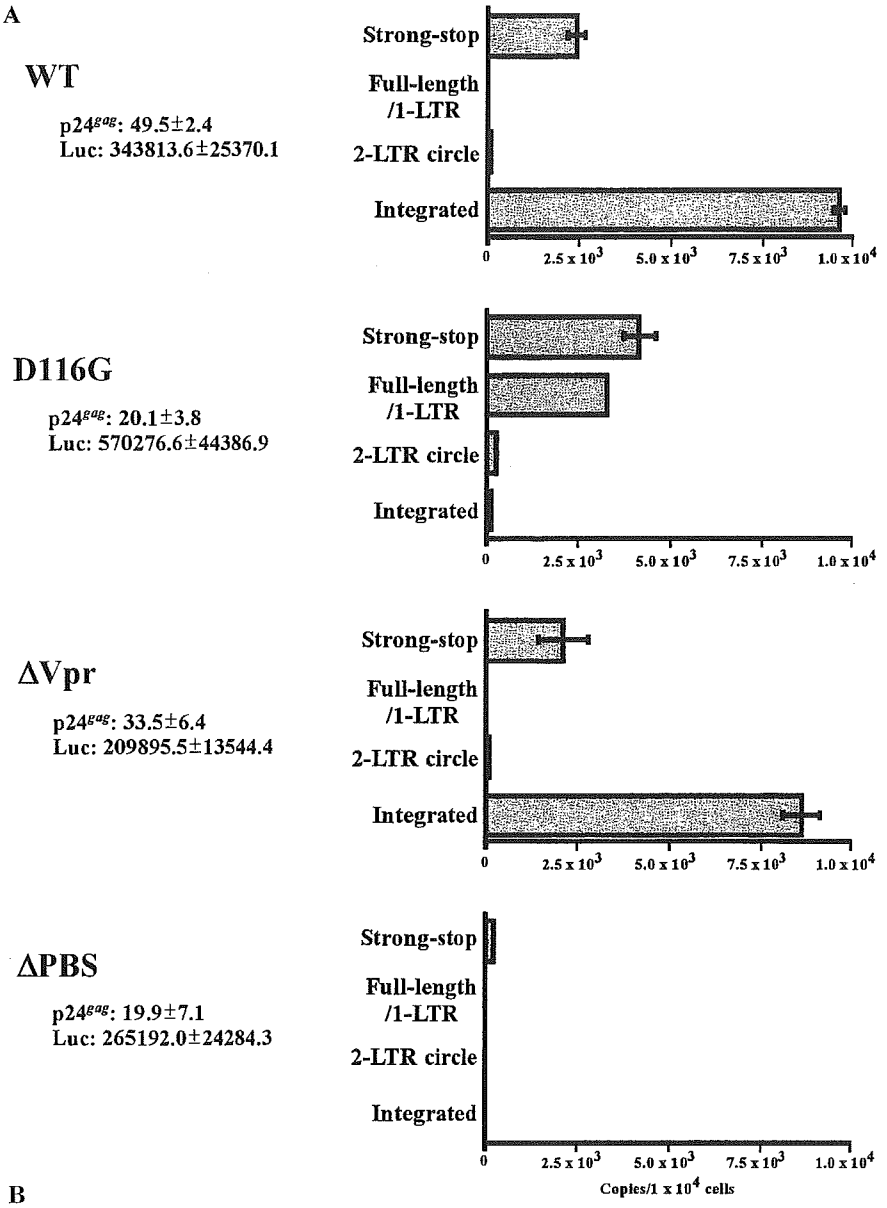
A
WT
p24gag: 49.5±2.4
Luc: 343813.6±25370.1
D116G
p24gag: 20.1±3.8
Luc: 570276.6±44386.9
ΔVpr
p24gag: 33.5±6.4
Luc: 209895.5±13544.4
ΔPBS
p24gag: 19.9±7.1
Luc: 265192.0±24284.3
Strong-stop
Full-length /1-LTR
2-LTR circle
Integrated
0
2.5 x 10^3
5.0 x 10^3
7.5 x 10^3
1.0 x 10^4
Copies/1 x 10^4 cells
B
WT
D116G
ΔVpr
ΔPBS
0
2 x 10^5
4 x 10^5
6 x 10^5
8 x 10^5
Luciferase activity (relative light units/mg protein)

integration has not been reported in nondividing cells. Therefore, using our real-time PCR assay, we finally investigated whether quiescent condition of PBMC has influence on the integration events of HIV-1. In this experiment, the PBMC cultures that had been stimulated with PHA and IL-2 (PHA-PBMC) and that had not been stimulated with exogenous mitogen (unstimulated PBMC) were infected with VSV-G-pseudotyped WT or ΔVpr. Cell-cycle analyses confirmed that efficient cell-cycle progression was observed in the infected PHA-PBMC culture, while that in the infected unstimulated culture was almost completely stopped at G_0/G_1, demonstrating that the majority of the cells in this culture were largely quiescent (Fig. 5A). DNA was then isolated 48 h after infection and subjected to the real-time PCR assay. In each infected cells, significant copies of viral DNA were detected by R/U5 specific primers (WT: 2,824.3 ± 133.9 copies and ΔVpr: 748.9 ± 129.8 copies in 1×10^5 cells of infected PHA-PBMC, WT: 1,190.5 ± 192.6 copies and ΔVpr: 535.6 ± 76.7 copies in 1×10^5 cells of infected unstimulated PBMC), demonstrating that sufficient amount of viruses entered into these PBMC cultures. Figure 5B shows the percent of integrated DNA in R/U5 DNA that indicates total viral DNA in infected cells (see Fig. 1). In PHA-PBMC culture, 35.3% and 25.2% of the total viral DNA were integrated forms with WT and ΔVpr infection, respectively (Fig. 5B). In unstimulated PBMC culture with WT infection the proportion of integrated DNA was not significantly reduced (24.7%, Fig. 5B). In contrast, significant lower level of the integrated DNA (3.0%) was detected in unstimulated PBMC with infection of ΔVpr (Fig. 5B). As expected, the percent of full-length DNA in infected unstimulated PBMC (34.8%) was clearly lower than that in infected PHA-PBMC (57.4%). Next, we compared the levels of integrated DNA per U5/gag DNA that indicates fully synthesized viral DNA by reverse transcription (Fig. 5C). Result showed that approximately 60% of the U5/gag

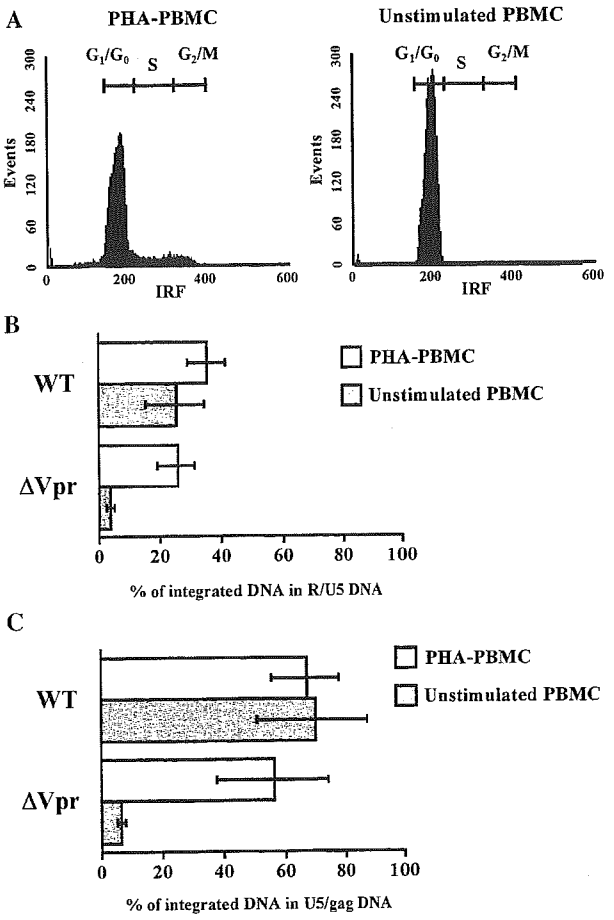

Fig. 5. Integration efficiency of WT and ΔVpr HIV-1 in stimulated or unstimulated PBMC culture. (A) Cell-cycle analysis of infected cells. The cells were harvested 48 h after infection, washed, fixed with 70% ethanol, and stained with propidium iodide followed by flow cytometer analysis. Integral red florescence (IRF) indicates the DNA content in the cell. (B) Proportion of integrated DNA in total viral DNA. DNA was extracted 48 h after infection and subjected to the real-time PCR assays using R/U5 primers for total viral DNA and *Alu*-HIV primers for integrated DNA. The percentages of the integrated DNA copies in the R/U5 DNA copies are indicated. (C) Proportion of integrated DNA in fully synthesized viral DNA. U5/gag DNA was detected as the fully synthesized viral DNA by real-time PCR assay and percent of integrated DNA copies per the U5/gag DNA copies are indicated. Results of (B) and (C) are means ± SD (error bar) from three independent experiments.

Fig. 4. Measurement of the individual forms of HIV-1 DNA in WT or mutant virus-infected cells. (A) The number of viral DNA copies per 1×10^4 cells is indicated (mean ± SD). The total DNA was extracted from MT-4 cells 48 h after infection, and 100 ng of DNA was subjected to the R/U5, U5/gag, 2-LTR and *Alu*-HIV PCR assays. To prepare each pseudotype virus, 293T cells were co-transfected with luciferase-expressing HIV-1 vector DNA and VSV-G-expressing DNA. The amount of HIV-1 $p24^{gag}$ in the culture supernatant (ng/ml) from transfected cells and the luciferase activity (Luc, relative light units/μg protein) in the transfected cells (3 days) are indicated as means ± SD. Results are from triplicate experiments. (B) Luciferase activity in WT- or mutant virus-infected cells. Cells were washed and resuspended in luciferase lysis buffer 48 h after infection and the luciferase activity was measured. The activities are indicated as the mean relative light units per microgram protein ± SD (error bar). Results are from three independent experiments.

DNA was integrated DNA in WT- and ΔVpr-infected PHA-PBMC (66.6% and 56.2%, respectively) and this efficiency was not significantly changed in unstimulated PBMC with WT infection (69.4%, Fig. 5C). This suggests that nuclear localization and subsequent integration steps of HIV-1 replication are not blocked in the quiescent condition. However, only 6.3% of the U5/gag DNA was detected as integrated forms in unstimulated PBMC with ΔVpr infection (Fig. 5C). Thus, our data clearly indicated that *vpr* gene is necessary for the provirus formation in quiescent cells.

Discussion

Accurate measurement of HIV-1 DNA, especially the integrated form, is useful for infection experiments and clinical samples. Measurement of the integrated HIV-1 DNA may be critical to know the level of the latent infection in patients under anti-retroviral therapy. So far, some PCR-based assays that can selectively detect and quantify the integrated DNA have been reported [11,13,31,32]. To measure the integrated DNA, we independently developed a quantitative assay by combination with *Alu*-HIV PCR [11] and real-time PCR [12]. The *Alu* elements are abundant among the numerous repeated sequences in the human genome and more than 10^6 copies are found in human chromosomal DNA [33]. Thus, part of integrated DNA in HIV-1-infected cells can be specifically amplified by PCR primers between the provirus and the *Alu* sequences that should be adjacent to these genomic sequences [11]. In addition to its high sensitivity (Fig. 3), the assay established in present study was specific for integration, since in integrase catalytic-site mutant virus, D116G-infected cells, minimal integration was detected (Fig. 4A). The integration efficiency of HIV-1 has been previously evaluated using a reporter gene expression system such as luciferase-expressing HIV-1 [21,34,35]. However, our data from Vpr-defective virus (ΔVpr)-infected cells indicated that the level of luciferase activity in infected cells did not always correspond with that of integration (Fig. 4). Because Vpr induces G_2/M phase arrest and apoptosis of the cells [36], the lower expression of the luciferase gene in WT-infected cells might be due to the cytopathogenic effects of the Vpr protein. Thus, our real-time PCR assay provides precise and direct information for characterizing the mutant HIV-1 in early phase of infection.

In this study, we also demonstrate an application of the real-time PCR assay for HIV-1-infected primary cells. It has been reported that Vpr protein is highly nucleophilic and likely contributes to nuclear localization of HIV-1 PIC [2,37–39], and the critical contribution of Vpr in viral replication has been well demonstrated in MDM [15,18,19,40]. In case of unstimulated PBMC infection, the effect of *vpr* gene on viral replication is controversial; one report has shown that the replication of Vpr-defective virus is extremely low [30], while the another study revealed that the viral replication in unstimulated PBMC culture is not affected by the lack of Vpr [18]. This inconsistency could be due to differences in preparation of cells, type of virus, or method to evaluate the viral replication. However, the influence of Vpr in provirus formation in infected PBMC has not been examined, which should have occurred after the nuclear translocation of viral DNA. We therefore examined by real-time PCR assay whether the integration step of Vpr-defective virus was really impaired in unstimulated PBMC culture. Our results directly revealed that the formation of the integrated DNA in unstimulated PBMC was dramatically reduced in the absence of Vpr (Fig. 5). Surprisingly, in WT virus-infected cells, approximately 25% of total viral DNA was integrated into chromosome even under the quiescent condition (Fig. 5B). Although some studies have reported that unstimulated PBMC is resistant to HIV-1 and SIV infection [29,41], this inconsistency might be explained by the poor transcription and translation activities in the quiescent cells. Indeed, the luciferase activity of WT virus was 25 times lower in unstimulated PBMC than in PHA-PBMC (data not shown).

It is well known that the post entry steps of the HIV-1 infection are blocked before the execution of further steps of viral replication in quiescent T lymphocytes or macrophages [8,10,17]. This has been demonstrated by impairing reverse transcription in the nondividing cells [10,17]. Also in our experiment, the inefficient reverse transcription was observed in unstimulated PBMC culture (see results). Then, is there any blockade after the completion of reverse transcription under the quiescent environment? The data from the comparison of integrated DNA per U5/gag DNA revealed that more than half of fully synthesized viral DNA was in integrated

form in WT-infected PHA-PBMC, and interestingly, the integration was not impaired in unstimulated PBMC (Fig. 5C), suggesting that once full-length DNA is synthesized, the further steps of the viral DNA are not blocked in quiescent condition. However, this efficiency was severely impaired in the absence of Vpr (Fig. 5C). Therefore, this result strongly suggests the critical contribution of Vpr for nuclear localization and subsequent integration of HIV-1 DNA. In addition, the effective conversion from full-length DNA to integrated DNA is remarkable, since in *in vitro* integration activity assay using PIC fraction from retrovirus-infected cells, the integration efficiency is approximately 30% [42–44]. Although two cellular proteins, BAF and HMG have been reported as components to stimulate the integration activity of HIV-1 PIC *in vitro* [4,5], another unknown factor might be involved in the integration step of HIV-1 *in vivo*.

Here, we reported the utility of real-time PCR assay to evaluate HIV-1 DNA dynamics *in vivo*. In all experiments, we used a VSV-G-pseudotyped HIV-1 infection system to detect a sufficient amount of viral DNA and determine the efficiency of reverse transcription and integration in single round of infection. However, because of the high sensitivity and specificity, our assay should be applicable to conventional HIV-1 infection. Therefore, further studies using this assay would provide us detailed information about the early phase of infection and novel strategies for blocking the HIV infection.

Acknowledgments

We thank I. Verma for providing the pCS-CG and I. Chen for the pNL43lucΔenv DNA. We also thank J. Burn and T. Friedmann for the pHCMVG and D. Trono for the pCMVΔR8.2 DNA.

This work was supported by grants from the Ministry of Health, Labor, and Welfare and by Priority Areas from the Ministry of Education, Culture, Sports, Science, and Biochemistry of Technology in Japan. Y.K. was supported by the Naito Foundation.

References

1. Flint S.J., Enquist J.W., Krug R.M., Racaniello V.R., and Skalka A.M., *Principles of Virology*, American Society of Microbiology, Washington, DC, 2000, pp. 199–234.
2. Heinzinger N.K., Bukinsky M.I., Haggerty S.A., Ragland A.M., Kewalramani V., Lee M.A., Gendelman H.E., Ratner L., Stevenson M., and Emerman M., Proc Natl Acad Sci USA *91*, 7311–7315, 1994.
3. Miller M.D., Farnet C.M., and Bushman F.D., J Virol *71*, 5382–5390, 1997.
4. Chen H. and Engelman A., Proc Natl Acad Sci USA *95*, 15270–15274, 1998.
5. Farnet C.M. and Bushman F.D., Cell *88*, 483–492, 1997.
6. Sharkey M.E., Teo I., Greenough T., Sharova N., Luzuriaga K., Sullivan J.L., Bucy R.P., Kostrikis L.G., Haase A., Veryard C., Davaro R.E., Cheeseman S.H., Daly J.S., Bova C., Ellison R.T., III Mady B., Lai K.K., Moyle G., Nelson M., Gazzard B., Shaunak S., and Stevenson M., Nat Med *6*, 76–81, 2000.
7. Kim S.Y., Byrn R., Groopman J., and Baltimore D., J Virol *63*, 3708–3713, 1989.
8. Schmidtmayerova H., Alfano M., Nuovo G., and Bukrinsky M., J Virol *72*, 4633–4642, 1998.
9. Pang S., Koyanagi Y., Miles S., Wiley C., Vinters H.V., and Chen I.S., Nature *343*, 85–89, 1990.
10. Zack J.A., Arrigo S.J., Weitsman S.R., Go A.S., Haislip A., and Chen I.S., Cell *61*, 213–222, 1990.
11. Chun T.W., Stuyver L., Mizell S.B., Ehler L.A., Mican J.A., Baseler M., Lloyd A.L., Nowak M.A., and Fauci A.S., Proc Natl Acad Sci USA *94*, 13193–13197, 1997.
12. Heid C.A., Stevens J., Livak K.J., and Williams P.M., Genome Res *6*, 986–994, 1996.
13. Butler S.L., Hansen M.S., and Bushman F.D., Nat Med *7*, 631–634, 2001.
14. Lewin S.R., Vesanen M., Kostrikis L., Hurley A., Duran M., Zhang L., Ho D.D., and Markowitz M., J Virol *73*, 6099–6103, 1999.
15. Tsurutani N., Kubo M., Maeda Y., Ohashi T., Yamamoto N., Kannagi M., and Masuda T., J Virol *74*, 4795–4806, 2000.
16. Fear W.R., Kesson A.M., Naif H., Lynch G.W., and Cunningham A.L., J Virol *72*, 1334–1344, 1998.
17. Sonza S., Maerz A., Deacon N., Meanger J., Mills J., and Crowe S., J Virol *70*, 3863–3869, 1996.
18. Connor R.I., Chen B.K., Choe S., and Landau N.R., Virology *206*, 935–944, 1995.
19. Freed E.O., Englund G., and Martin M.A., J Virol *69*, 3949–3954, 1995.
20. Harada S., Koyanagi Y., and Yamamoto N., Science *229*, 563–566, 1985.
21. Masuda T., Planelles V., Krogstad P., and Chen I.S., J Virol *69*, 6687–6696, 1995.
22. Akkina R.K., Walton R.M., Chen M.L., Li Q.X., Planelles V., and Chen I.S., J Virol *70*, 2581–2585, 1996.
23. Kawano Y., Tanaka Y., Misawa N., Tanaka R., Kira J.I., Kimura T., Fukushi M., Sano K., Goto T., Nakai M., Kobayashi T., Yamamoto N., and Koyanagi Y., J Virol *71*, 8456–8466, 1997.
24. Adachi A., Gendelman H.E., Koenig S., Folks T., Willey R., Rabson A., and Martin M.A., J Virol *59*, 284–291, 1986.
25. Miyoshi K., Blomer U., Takahashi M., Gage F.H., and Verma I.M., J Virol *72*, 8150–8157, 1998.
26. Naldini L., Blomer U., Gage F.H., Trono D., and Verma I.M., Proc Natl Acad Sci USA *93*, 11382–11388, 1996.

27. Folks T.M., Clouse K.A., Justement J., Rabson A., Duh E., Kehrl J.H., and Fauci A.S., Proc Natl Acad Sci USA *86*, 2365–2368, 1989.
28. Beerens N., Klaver B., and Berkhout B., J Virol *74*, 2227–2238, 2000.
29. Kimata J.T., Mozaffarian A., and Overbaugh J., J Virol *72*, 245–256, 1998.
30. Shapiro S.Z., Maudru T., and Peden K.W., J Gen Virol *80*, 857–861, 1999.
31. O'Doherty U., Swiggard W.J., Jeyakumar D., McGain D., and Malim M.H., J Virol *76*, 10942–10950, 2002.
32. Vandegraaff N., Kumar R., Burrell C.J., and Li P., J Virol *75*, 11253–11260, 2001.
33. Stevens S.W. and Griffith J.D., Proc Natl Acad Sci USA *91*, 5557–5561, 1994.
34. Masuda T., Kuroda M.J., and Harada S., J Virol *72*, 8396–8402, 1998.
35. Planelles V., Bachelerie F., Jowett J.B., Haislip A., Xie Y., Banooni P., Masuda T., and Chen I.S., J Virol *69*, 5883–5889, 1995.
36. Stewart S.A., Poon B., Jowett J.B., and Chen I.S., J Virol *71*, 5579–5592, 1997.
37. Fouchier R.A. and Malim M.H., Adv Virus Res *52*, 275–299, 1999.
38. Popov S., Rexach M., Zybarth G., Reiling N., Lee M.A., Ratner L., Lane C.M., Moore M.S., Blobel G., and Bukrinsky M., Embo J *17*, 909–917, 1998.
39. Sherman M.P., de Noronha C.M., Heusch M.I., Greene S., and Greene W.C., J Virol *75*, 1522–1532, 2001.
40. Balliet J.W., Kolson D.L., Eiger G., Kim F.M., McGann K.A., Srinivasan A., and Collman R., Virology *200*, 623–631, 1994.
41. Mwaengo D.M. and Novembre F.J., J Virol *72*, 8976–8987, 1998.
42. Fujiwara T. and Mizuuchi K., Cell *54*, 497–504, 1988.
43. Lee M.S. and Craigie R., Proc Natl Acad Sci USA *91*, 9823–9827, 1994.
44. Li L., Farnet C.M., Anderson W.F., and Bushman F.D., J Virol *72*, 2125–2131, 1998.

Rapid Communication

J. Biochem. **134**, 637–639 (2003)
DOI: 10.1093/jb/mvg200

Role of the Zinc Fingers of HIV-1 Nucleocapsid Protein in Maturation of Genomic RNA

Seiki Baba[1], Ken-ichi Takahashi[*,1], Yoshio Koyanagi[2], Naoki Yamamoto[3], Hiroshi Takaku[1], Robert J. Gorelick[4] and Gota Kawai[†,1]

[1]Department of Industrial Chemistry, Faculty of Engineering, Chiba Institute of Technology, 2-17-1 Tsudanuma, Narashino-shi, Chiba 275-0016; [2]Department of Virology, Tohoku University School of Medicine, 2-1 Seiryou-machi, Aoba-ku, Sendai 980-8575; [3]Department of Molecular Virology, Faculty of Medicine, Tokyo Medical and Dental University, 1-5-45 Yushima, Bunkyo-ku, Tokyo 113-8519; and [4]dAIDS Vaccine Program, SAIC Frederick, Inc., NCI at Frederick, Frederick, Maryland 21702, USA

Received September 1, 2003; accepted September 25, 2003

The nucleocapsid protein of HIV-1 consists of two basic amino acid regions and two zinc fingers. We investigated the requirement of these domains for the structural conversion of a 39mer RNA covering the dimerization initiation site by using three peptides; wild-type NCp7, a mutant in which the two zinc fingers are mutated, and another mutant in which the two zinc fingers are deleted. The two mutants exhibited similar conversion activities to each other, which were lower than that of the wild-type, indicating that the two basic regions exhibit some activity for RNA chaperone, as we suggested before, and the zinc fingers enhance the efficiency of this activity.

Key words: DIS, HIV-1, maturation, nucleocapsid protein, zinc finger.

Abbreviations: HIV-1, human immunodeficiency virus type 1; DIS, dimerization initiation site; NC, nucleocapsid protein.

One of the functions of the nucleocapsid protein (NC) of human immunodeficiency virus type-1 (HIV-1) is as an RNA chaperone, which assists RNA molecules into their thermodynamically most stable conformation (*1*). NC consists of 55 amino acids (pNL4-3 sequence), of which basic residues, Arg and Lys, account for 27%. Another role of NC is in the recognition of genomic RNA during the assembly process (*2–5*). NC consists of two basic regions and two zinc fingers, as shown in Fig. 1A. A number of experiments have been performed to understand the role of the zinc fingers as well as the basic regions, and some of the results are summarized in Laughrea *et al.* 2001 (*6*). For example, mutations in the basic regions as well as the zinc fingers were found to inhibit the annealing of $tRNA^{Lys}_3$ to the primer binding site, whereas most site directed mutations, except for the distal (C-terminal) zinc finger, were silent as to genomic RNA dimerization. In contrast, the proximal (N-terminal) zinc finger was critically required for genomic RNA packaging. Recently, the CCHC fingers were found to be required for efficient nucleic acid chaperone activity including minus- and plus-strand transfer processes, as determined using a mutant NC having SSHS sequences instead of the native CCHC fingers (Fig. 1B) (*7*), and by using CCHH or CCCC NC mutants (*8*). On the other hand, the two basic regions of NC (Fig. 1C) can act as an RNA chaperone by converting the dimeric form of a 39mer RNA corresponding to the dimerization initiation site (Fig. 2) (*9*). It is difficult to compare these apparently contradictory results because the experiments were performed with different systems and conditions. Thus, it is important to compare the function with same system and conditions to examine the role of zinc fingers in the RNA chaperone activity of NC.

To examine the RNA chaperone activity of NC, we used the experimental system of a 39mer RNA (DIS39) covering the whole DIS sequence (*10*). DIS39 forms two types of dimers, the kissing-loop and extended-duplex dimers (Fig. 2), whose base pairing topologies have been confirmed by NMR analysis (*11*). They can be readily discriminated on PAGE: both dimers retain their dimeric states on electrophoresis through polyacrylamide gels containing Mg^{2+}. However, on PAGE without Mg^{2+}, the kissing-loop dimer separates into monomers, whereas the extended-duplex dimer remains in the dimeric state, because of their different Mg^{2+}-dependent stabilities. As reported in the previous paper, DIS39 mostly forms the kissing-loop dimer by itself at 37°C (Fig. 3, lanes 1 and 12) and is converted into the extended-duplex dimer when incubated at 55°C (lane 11).

We prepared three peptides, NCp7wt, NCp7-SSHS/SSHS and NCBR[1+2], which correspond to NCp7 of the pNL4-3 sequence, a mutant NCp7 having two SSHS sequences instead of the two CCHC zinc fingers, and the two basic regions of NCp7 of the LAV strain linked with two glycine residues (Fig. 1). DIS39 was converted into the extended-duplex dimer when incubated with equivalent or more NCp7wt at 37°C (Fig. 3, lanes 2–4). On the other hand, NCp7-SSHS/SSHS and NCBR[1+2] showed chaperone activities that were nearly identical and lower than that of NCp7wt (Fig. 3, lanes 5–7 and 8–10). This result indicates that the two basic regions surrounding

*Present address: Department of Bioscience, Faculty of Bioscience, Nagahama Institute of Bio-Science and Technology, 1266 Tamura-cho, Nagahama, Shiga 526-0829.
†To whom correspondence should be addressed. Tel/Fax: +81-47-478-0425, E-mail: gkawai@ic.it-chiba.ac.jp

© 2003 The Japanese Biochemical Society.

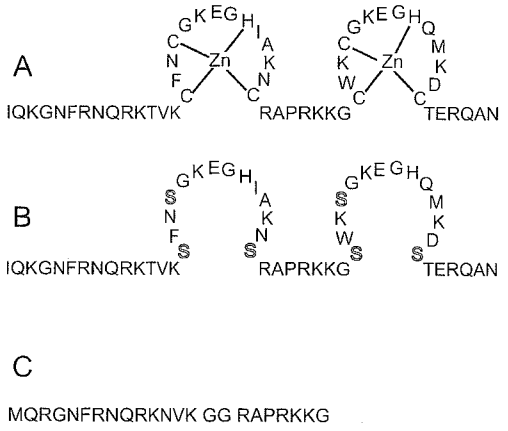

Fig. 1. **Peptide sequences of NCp7wt, NCp7-SSHS/SSHS and NCBR[1+2].** NCp7wt corresponds to NCp7 of the pNL4-3 sequence (A). NCp7-SSHS/SSHS has two SSHS sequences instead of the two CCHC zinc fingers of NCp7wt (B). NCBR[1+2] comprises the two basic regions of NCp7 of the LAV strain linked with two glycine residues (C). Recombinant NCp7wt and NCp7-SSHS/SSHS were expressed and purified as described previously (*7*, *17*, *18*). Synthetic peptide NCBR[1+2] was purchased from Sawady Technology (Tokyo).

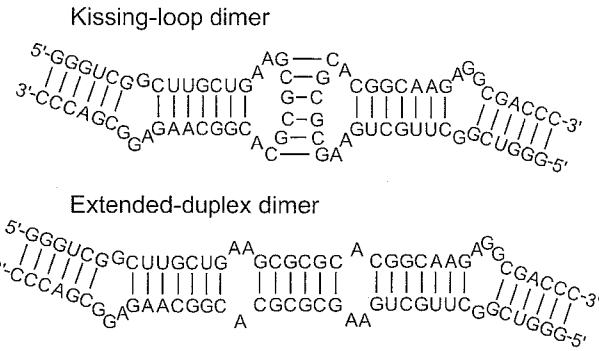

Fig. 2. **RNA sequence of a 39mer RNA corresponding to the dimerization initiation site (DIS39).** DIS39 forms two types of dimers, the kissing-loop and extended-duplex dimers, and NCp7 assists this conversion. RNA samples were synthesized enzymatically by *in vitro* transcription with AmpliScribe T7 Transcription Kits (Epicentre Technologies, WI, USA). Purification was performed by PAGE using 30 cm × 40 cm glass plates (Nihon Eido, Tokyo) under denaturing conditions, and extensive desalting by ultrafiltration (Centricon YM3., Amicon, MA, USA) was carried out.

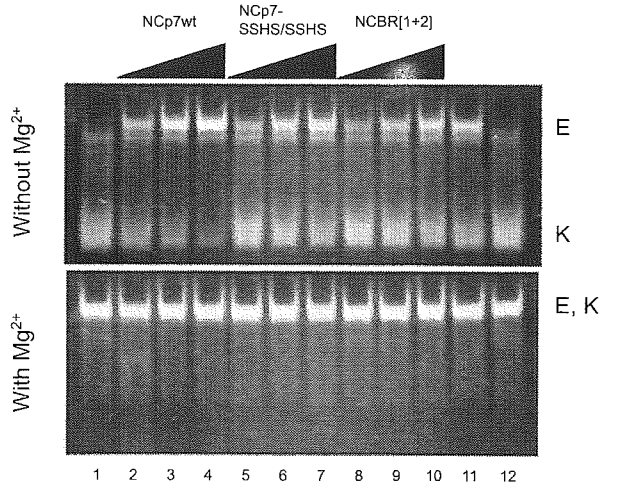

Fig. 3. **Assay for conformational conversion of DIS39 by NCp7wt, NCp7-SSHS/SSHS and NCBR[1+2].** Samples were incubated for 2.5 h at 37°C (lanes 1 to 10 and 12) or 55°C (lane 11). DIS39 was incubated alone (lanes 1, 11 and 12), or with 1, 2 and 3 equivalents of NCp7wt (lanes 2, 3 and 4, respectively), NCp7-SSHS/SSHS (lanes 5, 6 and 7, respectively) and NCBR[1+2] (lanes 8, 9 and 10, respectively). In the absence of Mg^{2+}, the kissing-loop dimer (K) separates into monomers, whereas the extended-duplex dimer (E) retains the dimeric state during electrophoresis through polyacrylamide gels. Both dimers retain their dimeric states in the presence of Mg^{2+}. The assay was performed as follows. After heating 12 μM DIS39 in 4 μl of water at 95°C for 5 min, it was chilled on ice for 5 min. Then 4 μl of 2 × PN buffer (1 × PN buffer contains 10 mM sodium phosphate [pH 7.0] and 50 mM NaCl) was added. After various concentrations of NCp7wt or its related peptides in 12 μl of 1 × PN buffer had been added, the RNA solutions were incubated at 37°C for 2.5 h and then treated with a phenol/chloroform solution regardless of the presence or absence of a peptide. Ten μl of the aqueous layer containing RNA was collected and mixed with 10 μl of loading buffer containing glycerol, and bromphenol and xylene cyanol dyes. The solution was then divided in two, which were separately analyzed by electrophoreses through nondenaturing polyacrylamide gels (10%) in TBM buffer (89 mM Tris, 89 mM borate, 1 mM $MgCl_2$) and TBE buffer (89 mM Tris, 89 mM borate, 2 mM EDTA), respectively, at room temperature. After electrophoresis the gels were stained with RedStain (BioRad Laboratories, CA, USA) and the RNA was visualized with an ultraviolet illuminator (FASIII., Toyobo, Osaka).

the N-terminal zinc finger has the RNA chaperone activity of NCp7 by themselves.

Although the NCp7wt sample used in the present study contained Zn^{2+} to prevent the formation of extended disulfide bridges within and among the molecules, we demonstrated that Zn^{2+} is not required for the efficient annealing activity in the DIS39 system in the previous study (*10*). Judging from the above together with the finding that NCp7-SSHS/SSHS and NCBR[1+2] still have annealing activity, the two zinc fingers might be important for defining the structural arrangement of the two basic regions in the case of the DIS39 system. Probably, the two basic regions in NCp7-SSHS/SSHS and NCBR[1+2] cannot form the optimized arrangement of the basic regions and/or residues for the chaperone activity. Some mutations in the basic regions as well as the zinc fingers, but not the zinc coordinating residues decrease the RNA chaperone activity for $tRNA^{Lys}_3$ annealing (*6*, *12*). This may also be due to the disruption of the optimized arrangement of the basic regions and/or residues. Probably because the process of conversion of genomic RNA dimeric forms is simpler than that of $tRNA^{Lys}_3$ annealing, the effects of mutations on the dimerization are less drastic than these on the $tRNA^{Lys}_3$ annealing.

The NC domain of the Gag polyprotein has been found to tightly bind to the genomic RNA dimer via SL2 and SL3 stem-loops just downstream of the DIS (SL1) region (*3*, *13*). Thus, during virus particle formation, the zinc fingers are involved in recognizing the genomic RNAs in the first step and then, after cleavage of the Gag polyprotein (*14*, *15*), the basic regions of NCp7 induce the conformational change of the genomic RNA dimer, which is optimized by the presence of the zinc finger regions. The

present study showed that the DIS annealing activity, which reflects the conversion efficiency of the conformation of DIS, of NCp7 was also decreased to roughly 10% by the SSHS/SSHS mutation, judging from the band densities on the gel (Fig. 3). On the other hand, a previous study showed that the SSHS/SSHS mutation resulted in a <10% wild-type RNA content in the virus (*7*), suggesting a possible relation between the packaging of genomic RNAs and DIS annealing. It should be noted that deletion of the DIS (SL1) region also resulted in a 10% wild-type RNA content in the virus and the mutant virus exhibited 10% infectivity (unpublished results). Darlix *et al.* also suggested that RNA dimerization and packaging are related events (*5*, *13*), whereas Sakuragi *et al.* showed that dimerization can be dissociated from packaging (*16*). This possibility should be verified through future research.

GK wishes to thank Dr. Judith G. Levin for providing the authors the chance of this collaboration. This work was supported by the "Research for the Future" Program (JSPS-RFTF97L00503) of the Japan Society for the Promotion of Science, and by, in part, a Grant-in-Aid for High Technology Research from the Ministry of Education, Science, Sports and Culture, Japan, and, in part, federal funds from the National Cancer Institute, National Institutes of Health, under contract No. NO1-CO-12400 with SAIC-Frederick, Inc.

REFERENCES

1. Rein, A., Henderson, L.E., and Levin, J.G. (1998) Nucleic-acid-chaperone activity of retroviral nucleocapsid proteins: significance for viral replication. *Trends Biochem. Sci.* **23**, 297–301
2. de Guzman, R.N., Wu, Z.R., Stalling, C.C., Pappalardo, L., Borer, P.N., and Summers, M.F. (1998) Structure of the HIV-1 nucleocapsid protein bound to the SL3 Ψ-RNA recognition Element. *Science* **279**, 384–388
3. Amarasinghe, G.K., de Guzman, R.N., Turner, B.G., Chancellor, K.J., Wu, Z.R., and Summers, M.F. (2000) NMR structure of the HIV-1 nucleocapsid protein bound to Stem-Loop SL2 of the Ψ-RNA packaging signal. Implications for Genome recognition. *J. Mol. Biol.* **301**, 491–511
4. Berkowitz, R., Fisher, J., and Goff, S.P. (1996) RNA packaging. *Curr. Top. Microbiol. Immunol.* **214**, 177–218
5. Darlix, J.L., Lopez-Lastra, M., Mély, Y., and Roques, B. (2003) Nucleocapsid protein chaperoning of nucleic acids at the heart of HIV structure, assembly and cDNA synthesis in *HIV Sequence Compendium 2002* (Kuiken, C., Foley, B., Freed, E., Hahn, B., Marx, P., McCutchan, F., Mellors, J.W., Wolinsky, S., and Korber, B., eds.) pp. 69–88, Los Alamos National Laboratory, Los Alamos, NM
6. Laughrea, M., Shen, N., Jette, L., Darlix, J., Kleiman, L., and Wainberg, M.A. (2001) Role of distal zinc finger of nucleocapsid protein in genomic RNA dimerization of human immunodeficiency virus type 1; No role for the palindrome crowning the R-U5 hairpin. *Virology* **281**, 109–116
7. Guo, J., Wu, T., Anderson, J., Kane, B.F., Johnson, D.G., Gorelick, R.J., Henderson, L.E., and Levin, J.G. (2000) Zinc finger structures in the human immunodeficiency virus type 1 nucleocapsid protein facilitate efficient minus- and plus-strand transfer. *J. Virol.* **74**, 8980–8988
8. Guo, J., Wu, T., Kane, B.F., Johnson, D.G., Henderson, L.E., Gorelick, R.J., and Levin, J.G. (2002) Subtle alterations of the native zinc finger structures have dramatic effects on the nucleic acid chaperone activity of human immunodeficiency virus type 1 nucleocapcid protein. *J. Virol.* **76**, 4370–4378
9. Takahashi, K., Baba, S., Koyanagi, Y., Yamamoto, N., Takaku, H., and Kawai, G. (2001) Two basic regions of NCp7 are sufficient for conformational conversion of HIV-1 dimerization initiation site from kissing-loop dimer to extended-duplex dimer. *J. Biol. Chem.* **276**, 31274–31278
10. Takahashi, K., Baba, S., Chattopadhyay, P., Koyanagi, Y., Yamamoto, N., Takaku, H., and Kawai, G. (2000a) Structural requirement for the two-step dimerization of human immunodeficiency virus type 1 genome. *RNA* **6**, 96–102
11. Takahashi, K., Baba, S., Hayashi, Y., Koyanagi, Y., Yamamoto, N., Takaku, H., and Kawai, G. (2000b) NMR analysis of intra- and inter-molecular stems in the dimerization initiation site of the HIV-1 genome. *J. Biochem.* **127**, 681–686
12. Remy, E., Rocquigny, H., Petitjean, P., Muriaux, D., Theilleux, V., Paoletti, J., and Roques, B.P. (1998) The annealing of $tRNA^{Lys}_3$ to human immunodeficiency virus type 1 primer binding site is critically dependent on the NCp7 zinc fingers structure. *J. Biol. Chem.* **273**, 4819–4822
13. Darlix, J.L., Gabus, C., Nugeyre, M.T., Clavel, F., and Barre-Sinoussi, F. (1990) *Cis* elements and *trans*-acting factors involved in the RNA dimerization of the human immunodeficiency virus HIV-1. *J. Mol. Biol.* **216**, 689–699
14. Fu, W. and Rein, A. (1993) Maturation of dimeric viral RNA of moloney murine leukemia virus. *J. Virol.* **67**, 5443–5449
15. Fu, W., Gorelick, R.J., and Rein, A. (1994) Characterization of human immunodeficiency virus type 1 dimeric RNA from wild-type and protease-defective virions. *J. Virol.* **68**, 5013–5018
16. Sakuragi, J., Iwamoto, A., and Shioda, T. (2002) Dissociation of genome dimerization from packaging functions and virion maturation of human immunodeficiency virus type 1. *J. Virol.* **76**, 959–967
17. Carteau, S., Gorelick, R.J., and Bushman, F.D. (1999) Coupled integration of human immunodeficiency virus type 1 cDNA ends by purified integrase *in vitro*: Stimulation by the viral nucleocapsid protein. *J. Virol.* **73**, 6670–6679
18. Williams, M.C., Rouzina, I., Wenner, J.R., Gorelick, R.J., Musier-Forsyth, K., and Bloomfield, V.A. (2001) Mechanism for nucleic acid chaperone activity of HIV-1 nucleocapsid protein revealed by single molecule stretching. *Proc. Natl Acad. Sci. USA* **98**, 6121–6126

ELSEVIER

Journal of Neuroimmunology 151 (2004) 189–194

Journal of
Neuroimmunology

www.elsevier.com/locate/jneuroim

Short communication

Th1/Th2 balance and HTLV-I proviral load in HAM/TSP patients treated with interferon-α

Juan Feng[a], Tatsuro Misu[a], Kazuo Fujihara[a,*], Naoko Misawa[b], Yoshio Koyanagi[b], Yusei Shiga[a], Atsushi Takeda[a], Shigeru Sato[c], Sadao Takase[c], Takeshi Kohnosu[d], Hiroshi Saito[d], Yasuto Itoyama[a]

[a] *Department of Neurology, Tohoku University School of Medicine 1-1 Seiryomachi, Aobaku, Sendai 980-8574, Japan*
[b] *Department of Microbiology, Tohoku University School of Medicine, Japan*
[c] *Department of Neurology, Kohnan Hospital, Japan*
[d] *Department of Neurology, National Nishitaga Hospital, Japan*

Received 6 October 2003; received in revised form 15 January 2004; accepted 20 February 2004

Abstract

We studied the immunological and virological effects of interferon-α (IFN-α) therapy in nine patients with HTLV-I-associated myelopathy (HAM/TSP). After therapy, the percentages of CCR5+ cells in CD4+ cells significantly decreased in the cerebrospinal fluid as well as blood. The therapy also significantly lowered the intracellular IFN-γ+/interleukin-4+ T-cell ratio in blood. Those helper T-cell type 1 (Th1)-related responses tended to be higher and reduce more evidently following therapy in three patients who clinically improved. Also, all the three patients had one or more HTLV-I copies in five blood mononuclear cells. These results suggest that IFN-α suppresses Th1 responses in HAM/TSP and that the patients with higher Th1 immunity and proviral loads may be responders of the therapy. Larger-scale studies are needed to confirm the findings.
© 2004 Elsevier B.V. All rights reserved.

Keywords: HAM/TSP; HTLV-I; Interferon-alpha therapy; Helper T cell; Chemokine receptor

1. Introduction

Human T-lymphotropic virus type I (HTLV-I) is associated with chronic inflammatory myelopathy, HTLV-I-associated myelopathy/tropical spastic paraparesis (HAM/TSP) (Gessain et al., 1985; Osame et al., 1986; Izumo et al., 2000). Previous studies demonstrated remarkable immune activation including helper T-cell type 1 (Th1)-associated responses (Kuroda and Matsui, 1993; Itoyama et al., 1996; Umehara et al., 1994; Jacobson et al., 1998) and high HTLV-I proviral loads (Nagai et al., 1998) in HAM/TSP. These immunological and virological changes are probably important in the pathogenesis of this myelopathy and effective immunotherapies for HAM/TSP need to suppress these abnormalities.

A randomized, double-blind study demonstrated that interferon-α (IFN-α) was clinically effective in HAM/TSP (Izumo et al., 1996). The immunological effects of the therapy had been unclear, but we recently found a significant reduction of CD4 cell subsets in the cerebrospinal fluid (CSF) of the patients receiving the therapy (Feng et al., 2003). Here, we report Th1 and Th2-associated chemokine receptor expression on T cells, intracellular cytokine levels in T cells and HTLV-I proviral loads in blood before and after the therapy in the same patients.

2. Materials and methods

2.1. Subjects

Nine patients (five women and four men) were enrolled in the present study as reported previously (Feng et al., 2003). Their ages ranged from 54 to 72 years old and the duration of disease was from 2 to 50 years. The clinical disability was graded according to the Osame's scale: motor

* Corresponding author. Tel.: +81-22-717-7189; fax: +81-22-717-7192.
E-mail address: fujikazu@em.neurol.med.tohoku.ac.jp (K. Fujihara).

0165-5728/$ - see front matter © 2004 Elsevier B.V. All rights reserved.
doi:10.1016/j.jneuroim.2004.02.007

disability: grade 0 (normal)–13 (bedridden), dysuria: grade 0 (normal)–3 (severe) (Izumo et al., 1996). The patients received intramuscular injections of IFN-α (3 million units) daily for 4 weeks (Izumo et al., 1996). None had received immunosuppressants for the last 3 months except for a single patient (HAM3) who was treated with a fixed dose of oral prednisolone (20 mg/day) throughout the therapy. Age- and sex-matched nine HTLV-I-seronegative control subjects were studied for peripheral blood mononuclear cells (PBMC). We obtained informed consents prior to the study and the present study conformed to the guidelines of Medical Ethics Committee of our medical school.

2.2. Mononuclear cell preparation

Heparinized venous blood and CSF were collected before the IFN-α therapy and the next day of the last IFN-α injection. PBMC were isolated by Ficoll-Paque and CSF cells were directly isolated by centrifugation.

2.3. Flow cytometric analysis

2.3.1. T-cell subset

We analyzed T-cell subsets using a standard direct immunofluorescent technique with monoclonal antibodies (MoAbs), a three-color flow cytometer (FACSCalibur, Becton Dickinson, San Jose, CA) and the CellQuest software.

The analyzed subsets were CCR5+ and CXCR3+ (helper T-cell type 1 [Th1]-associated chemokine receptor expressing cells) and CCR3+ (Th2-associated chemokine receptor expressing cells, especially in the early stage of Th2 response) among CD4+ and CD8+ cells. Peridinin chlorophyll protein-conjugated anti-CD4 and anti-CD8, fluorescein isothiocyanate-conjugated anti-CD8 MoAbs were provided by Becton Dickinson. Phycoerythrin-conjugated anti-CCR5 and anti-CCR3 and carboxy-fluorescein succinimidylester-conjugated anti-CXCR3 MoAbs were purchased from Dako (Tokyo, Japan).

The data were expressed as the percentages of T-cell subsets in CD4+ or CD8+ cells.

2.3.2. Intracellular Th1/Th2-associated cytokines

The ratio of IFN-γ producing cells to interleukin-4 (IL-4) producing cells in CD3+ cells was assayed with a FACSCalibur according to the previous report (Pala et al., 2000).

2.4. HTLV-I proviral load in PBMC

DNA was extracted from PBMC. The HTLV-I proviral load was quantified using a real-time Taq-Man PCR method (PE Applied Biosystems, Foster City, CA). Standard curves of β-actin and HTLV-I tax genes were generated using DNA derived from an HTLV-I infected cell line, TloM1. TaqMan amplifications were carried out with the forward primers 5′-ACTCCTCAAGCGAGCTGCAT-3′, the reverse primer 5′-TTTTTCTTTGGGATCGGCG-3′ (Greiner Japan, Tokyo, Japan) and HTLV-I TaqMan Probe 5′-CCCAAGACCC-GTCGGAGGCC-3′ labeled with the 5′ FAM reporter dye and the 3′ TAMRA quencher dye molecules (Japan BioService, Asaka, Japan). The primers and probe for β-actin gene were obtained from PE Applied Biosystems. The thermal cycle conditions were 50 °C for 2 min followed by 95 °C for 10 min (hot start) and then 40 cycles were run by melting at 95 °C for 15 s and annealing/extension at 60 °C for 1 min in each cycle. Each sample was analyzed in triplicate. For each reaction, 100 ng of DNA, the equivalent of 2×10^4 cells, were subjected to the analysis. The amplifications were performed on an ABI PRISM 7700 sequence detector equipped with a 96-well thermal cycler. Copy numbers were reported as copy equivalents per 10^5 PBMC.

2.5. Statistical analysis

We used Mann–Whitney *U*-test to compare the unpaired values, Wilcoxon's signed rank test to compare the paired values. We also examined correlations in clinical disability, immunological and virological parameters (motor disability grade, percentages of CCR5+, CXCR3+ and CCR3+ in CD4+ cells, and CCR5+, CXCR3+ and CCR3+ in CD8+ cells in the CSF and blood, ratio of IFN-γ producing cells to IL-4 producing cells in blood CD3+ cells, and HTLV-I proviral load) of the HAM/TSP patients with Spearman rank correlation coefficient test. Correlations in both baseline values and the changes after the IFN-α therapy were analyzed. *P*-values less than 0.05 were considered statistically significant.

3. Results

3.1. Clinical effects

The motor disability grade improved in three patients after the IFN-α therapy (Patients HAM 3, grade 3 → 2; HAM 5, grade 8 → 6; HAM 6, grade 6 → 4) as we reported (Feng et al., 2003). The dysuria grade did not change.

3.2. T-cell subsets (Table 1)

3.2.1. CCR5

The percentage of CCR5+ cells in blood CD4+ cells was significantly higher before the IFN-α therapy in HAM/TSP than in control. In HAM/TSP, the mean percentages of all CCR5+ T-cell subsets in blood and CSF decreased after the therapy. Among them, the percentage of CCR5+ cells in blood CD4+ cells of HAM/TSP significantly decreased after the therapy, and they were no longer different between HSM/TSP and control. The percentage of CCR5+ cells in CSF CD4+ cells also significantly decreased after the therapy (Table 1).

Table 1
T cells expressing Th1/Th2-associated chemokine receptors in HAM/TSP patients treated with interferon-α and in control subjects

	CCR5+ in CD4+	CXCR3+ in CD4+	CCR3+ in CD4+
Control (n=9)	(%)	(%)	(%)
Blood	0.5 ± 0.1	27.3 ± 4.8	0.3 ± 0.1
HAM/TSP (n=9)			
Blood			
before IFN-α	1.5 ± 0.9 *	27.9 ± 12.3	0.3 ± 0.2
after IFN-α	0.9 ± 0.8 *	25.5 ± 7.6	0.4 ± 0.2
CSF			
before IFN-α	20.5 ± 8.8 *	88.5 ± 5.4	4.3 ± 4.3
after IFN-α	13.4 ± 5.3 *	81.3 ± 12.2	7.5 ± 3.1
	CCR5+ in CD8+	CXCR3+ in CD8+	CCR3+ in CD8+
Control (n=9)	(%)	(%)	(%)
Blood	0.9 ± 0.9	35.9 ± 8.1	0.5 ± 0.2
HAM/TSP (n=9)		*	
Blood			
before IFN-α	3.0 ± 4.5	55.5 ± 17.4 *	0.7 ± 0.4
after IFN-α	1.6 ± 1.0	36.4 ± 17.6 *	0.6 ± 0.2
CSF			
before IFN-α	27.1 ± 12.1	94.8 ± 4.4	4.3 ± 4.3
after IFN-α	17.9 ± 6.5	90.3 ± 9.3	7.5 ± 3.6

Data are mean percentages ± standard deviation.
*$P < 0.05$.

The percentage of CCR5+ cells in CSF CD4 cells was unequivocally higher in the three patients who clinically improved after the therapy (the lowest value was 26.8% in Patient HAM 6) than in the six patients without clinical effect (the highest value was 18.3% in Patient HAM 2).

3.2.2. CXCR3

In blood, the percentages of CXCR3+ cells in CD8+ cells were significantly higher in HAM/TSP before the therapy than in control. In HAM/TSP, the mean percentages of all CXCR3+ T-cell subsets in blood and CSF decreased after the therapy. Among them, the percentage of CXCR3+ cells in CD8+ cells significantly decreased after the therapy in HAM/TSP, and it was no longer different between HAM/TSP and control.

3.2.3. CCR3

No CCR3+ subset was significantly different between HAM/TSP and control or changed significantly after the therapy in HAM/TSP, although the mean percentages of CCR3+ cells in CSF CD4+ and CD8+ cells increased after the therapy.

3.3. Intracellular TH1/TH2-associated cytokines (Fig. 1)

The IFN-α therapy significantly decreased the ratio of intracellular IFN-γ- versus IL-4-producing T cells in blood (9.5 ± 7.6 before the therapy and 5.8 ± 4.9 after the therapy). The ratios in the three patients who clinically improved following the therapy (Patients HAM 3, 5 and 6) were over 5.0, while the therapy was not effective in any of the four patients with the ratios being less than 5.0 (Patients HAM 9, 4, 1 and 7).

3.4. HTLV-I proviral load (Fig. 2)

The HTLV-I proviral copy number before the IFN-α therapy in the nine patients was 13272 ± 9006 copies and

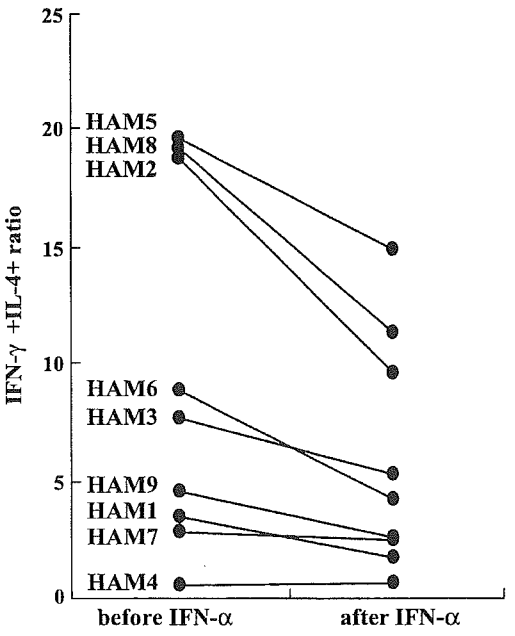

Fig. 1. Intracellular Th1/Th2 cytokine balance in T cells of the patients with HAM/TSP treated with IFN-α. The ratio of IFN-γ+ cells to IL-4+ cells among CD3+ T cells was significantly lower after the IFN-α therapy. Before-IFN-α, before IFN-α therapy; after-IFN-α, after IFN-α therapy.

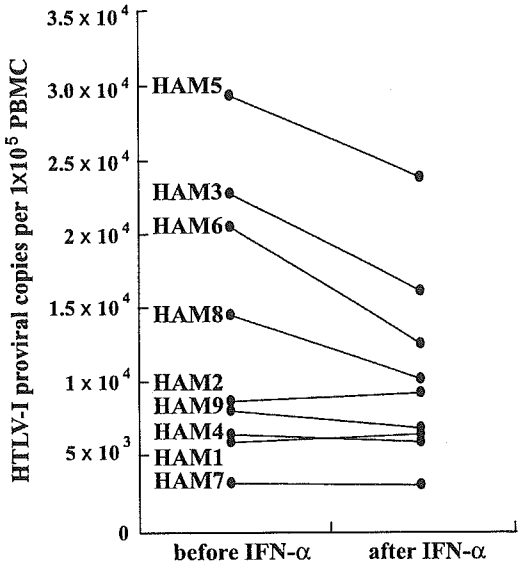

Fig. 2. HTLV-I proviral loads in the PBMC of the patients with HAM/TSP treated with IFN-α. After the IFN-α therapy, HTLV-I proviral loads apparently decreased in the patients with higher proviral loads, and clinical effect was seen in the three patients with 2×10^4 copies or more in 10^5 PBMC (HAM3, HAM5 and HAM6). Before-IFN-α, before IFN-α therapy; after-IFN-α, after IFN-α therapy.

that after the therapy was 10472 ± 6323 copies ($P = 0.06$). Patients HAM 3, 5, 8 and 6, who had the highest proviral loads and who experienced the most obvious decline in proviral load as a result of therapy, were among the ones with the highest baseline ratios of intracellular IFN-γ- versus IL-4-producing blood T cells and with the most dramatic decline in those values following the therapy (Fig. 1). Furthermore, three of these four patients were the ones who clinically improved, and all the three patients had 2×10^4 HTLV-I copies or more in 10^5 PBMC. Meanwhile, clinical effect was not seen in any patient with lower HTLV-I proviral load and their proviral loads remained unchanged after the therapy (Fig. 2).

3.5. Correlation

None of the correlations in clinical disability, immunological and virological parameters in the HAM/TSP patients was statistically significant.

3.6. Comparison of immunological and virological findings in responders and non-responders to IFN-α therapy

We compared the immunological and virological findings in responders (Patients HAM 3, 5 and 6) and non-responders (Patients HAM 1, 2, 4, 7, 8 and 9) to the IFN-α therapy (Table 2). We could not analyze the data statistically due to the small sample size. However, among the significant parameters in the statistical analyses of HAM/TSP patients, there was a tendency for the percentages of CCR5+ cells in CD4+ cells in the CSF and blood, the ratio of intracellular IFN-γ- versus IL-4-producing T cells in blood, and the HTLV-I proviral load to be higher and reduce more evidently following the therapy in responders as compared with non-responders. In the other parameters, the percen-

Table 2
Immunological and virological data in "responders" and "non-responders" to the interferon-α therapy

	CCR5+ in CD4+ (%)	CXCR3+ in CD4+ (%)	CCR3+ in CD4+ (%)	CCR5+ in CD8+ (%)	CXCR3+ in CD8+ (%)	CCR3+ in CD8+ (%)	IFN-γ/ IL-4 ratio	HTLV-1 proviral load (copies/10^5 PBMC)
Blood								
Responders								
(A) Before therapy	2.0 ± 1.1	28.7 ± 7.8	0.4 ± 0.1	5.6 ± 7.6	49.1 ± 21.2	0.5 ± 0.1	11.8 ± 6.1	24156 ± 4666
(B) After therapy	1.1 ± 0.3	23.3 ± 4.8	0.4 ± 0.2	2.1 ± 1.0	37.2 ± 17.4	0.6 ± 0.4	6.4 ± 2.9	17506 ± 5694
(A)−(B)	0.9 ± 0.4	6.4 ± 7.6	0.0 ± 0.1	3.5 ± 6.6	11.8 ± 4.0	0.1 ± 0.2	5.4 ± 3.5	6650 ± 1107
Non-responders								
(A) Before therapy	1.2 ± 0.8	26.1 ± 10.9	0.4 ± 0.1	1.7 ± 1.7	51.2 ± 19.0	0.8 ± 0.5	8.3 ± 8.7	7830 ± 3802
(B) After therapy	1.0 ± 1.0	26.0 ± 8.8	0.4 ± 0.1	1.3 ± 1.0	37.4 ± 17.6	0.5 ± 0.1	5.6 ± 5.9	6954 ± 2538
(A)−(B)	0.4 ± 0.2	2.4 ± 3.2	0.1 ± 0.2	0.5 ± 0.0	13.8 ± 10.1	0.2 ± 0.5	2.7 ± 3.0	876 ± 1851
CSF								
Responders								
(A) Before therapy	33.5 ± 9.0	92.7 ± 0.8	8.8 ± 5.7	35.4 ± 17.1	97.8 ± 3.1	6.1 ± 2.8		
(B) After therapy	19.4 ± 3.0	89.5 ± 3.2	9.0 ± 4.6	25.4 ± 19.7	96.8 ± 0.5	7.5 ± 1.4		
(A)−(B)	14.1 ± 5.9	3.1 ± 4.0	−0.2 ± 1.1	9.9 ± 19.0	1.0 ± 2.6	−1.5 ± 1.3		
Non-responders								
(A) Before therapy	15.3 ± 2.0	86.8 ± 5.6	2.1 ± 0.6	23.9 ± 9.9	93.6 ± 4.5	3.1 ± 2.9		
(B) After therapy	10.9 ± 4.0	78.0 ± 13.2	6.1 ± 0.2	15.9 ± 5.3	87.9 ± 9.0	7.6 ± 5.0		
(A)−(B)	4.2 ± 2.4	8.8 ± 17.4	−4.5 ± 0.4	8.9 ± 12.2	5.8 ± 11.2	−4.8 ± 6.2		

Data are shown as mean ± standard deviation.
IFN-γ, interferon-gamma; IL-4, interleukin-4; IFN-γ/IL-4, ratio of IFN-γ producing cells to IL-4 producing cells in CD3+ cells; PBMC, peripheral blood mononuclear cells; CSF, cerebrospinal fluid.

tages of CCR3+ cells in CSF CD4+ and CD8+ cells tended to be lower and increase more after the therapy in non-responders than in responders.

4. Discussion

Our previous analysis revealed a significant reduction of CD4+ cells in CSF of HAM/TSP after IFN-α therapy (Feng et al., 2003). In the present study, we focused on the Th1/Th2 balance and showed that IFN-α therapy significantly reduced CCR5 + CD4+ cells, a Th1 subset, in the patients' CSF as well as blood. The CCR5 + CD4+ cell subset in CSF reflects the disease activity in multiple sclerosis (Misu et al., 2001). This subset is increased in the synovium of active rheumatoid arthritis (Mack et al., 1999), and the inhibition of CCR5 successfully treated adjuvant arthritis in rats, an animal model of rheumatoid arthritis (Barnes et al., 1998). In HAM/TSP, elevated levels of CCR5 on memory CD4+ cells in PBMC (Wu et al., 2000) and macrophage inflammatory protein-1α, a CCR5 ligand, in CSF (Miyagishi et al., 1995) were reported. These findings suggest a pathogenic role of CCR5 + CD4+ cells in HAM/TSP and other immunologic diseases, and a suppression of the subset by IFN-α might relate to the alleviation of myelitis in HAM/TSP.

There was also a tendency for the CXCR3 + CD4 cell, another Th1 subset, to be decreased and CCR3 + CD4+ cells, a Th2 subset, to be increased in CSF of the treated patients. A significant decrease in blood CD8+ cell number in the treated patients (Feng et al., 2003) may be attributable to the reduction in CXCR3 + CD8+ cells. Moreover, intracellular Th1/Th2-associated cytokine ratio in T cells, which was analyzed only in blood because of the limited volumes of CSF, reduced significantly following the therapy. Taken together, our data suggests that the IFN-α therapy suppressed Th1-related responses in HAM/TSP, although our small-scale study did not address whether the immunological changes were directly associated with the clinical efficacy of IFN-α in HAMTSP.

The present study suggested some interesting differences in baseline immunological and virological findings between responders and non-responders to the IFN-α therapy, that is, responders showed higher Th1 responses and more viral replication than non-responders, and the therapeutic suppression to those parameters was more evident in responders. Our small-scale study could not confirm the associations statistically, but those analyses will be critically important to reliably predict therapeutic efficacy of intramuscular injections of IFN-α beforehand. Whether such laboratory data as (1) baseline percentage of CCR5+ cells in CSF CD4+ cells >20%, (2) baseline ratio of intracellular IFN-γ- versus IL-4-producing blood T cells >5.0 and (3) baseline HTLV-I proviral load more than one copy in five PBMC are really linked to clinical efficacy of IFN-α therapy in HAM/TSP need to be examined in a larger cohort of patients by statistical analyses.

Acknowledgements

The authors thank Mr. Brent Bell for reading the manuscript. This work was supported by the grants from the Ministry of Education, Science, Culture, Sports and Technology and the Tawara's Endowment for HAM Research.

References

Barnes, D.A., Tse, J., Kaufhold, M., Owen, M., Hesselgesser, J., Strieter, R., Horuk, R., Perez, H.D., 1998. Polyclonal antibody directed against human RANTES ameliorates disease in the Lewis rat adjuvant-induced arthritis model. J. Clin. Invest. 101, 2910–2919.

Feng, J., Misu, T., Fujihara, K., Saito, H., Takahashi, T., Kohnosu, T., Shiga, Y., Takeda, A., Sato, S., Takase, S., Itoyama, Y., 2003. Interferon-alpha significantly reduces cerebrospinal fluid CD4 cell subsets in HAM/TSP. J. Neuroimmunol. 141, 170–173.

Gessain, A., Barin, F., Vernant, J.C., Gout, O., Maurs, L., Calender, A., de The, G., 1985. Antibodies to human T-lymphotropic virus type-I in patients with tropical spastic paraparesis. Lancet 2, 407–410.

Itoyama, Y., Kira, J., Fujii, N., Goto, I., Yamamoto, N., 1996. Increases in helper inducer T cells and activated T cells in HTLV-I-associated myelopathy. Ann. Neurol. 26, 257–262.

Izumo, S., Goto, I., Itoyama, Y., Okajima, T., Watanabe, S., Kuroda, Y., Araki, S., Mori, M., Nagataki, S., Matsukura, S., Akamine, T., Nakagawa, M., Yamamoto, I., Osame, M., 1996. Interferon-alpha is effective in HTLV-I-associated myelopathy: a multicenter, randomized, double-blind, control trial. Neurology 46, 1016–1021.

Izumo, S., Umehara, F., Osame, M., 2000. HTLV-I-associated myelopathy. Neuropathology 20, S65–68 (Suppl).

Jacobson, S., Levin, M., Utz, U., Drew, P., 1998. Infectious immune disorders: HTLV-I. In: Antel, J.P., Birnbaum, G., Hartung, H.P. (Eds.), Clinical neuroimmunology. Blackwell, Malden, pp. 204–217.

Kuroda, Y., Matsui, M., 1993. Cerebrospinal fluid interferon-gamma is increased in HTLV-I-associated myelopathy. J. Neuroimmunol. 42, 223–236.

Mack, M., Bruhl, H., Gruber, R., Jaeger, C., Cihak, J., Eiter, V., Plachy, J., Stangassinger, M., Uhlig, K., Schattenkirchner, M., Schlondorff, D., 1999. Predominance of mononuclear cells expressing the chemokine receptor CCR5 in synovial effusions of patients with different forms of arthritis. Arthritis Rheum. 42, 981–988.

Misu, T., Onodera, H., Fujihara, K., Matsushima, K., Yoshie, O., Okita, N., Takase, S., Itoyama, Y., 2001. Chemokine receptor expression on T cells in blood and cerebrospinal fluid at relapse and remission of multiple sclerosis: imbalance of Th1/Th2-associated chemokine signaling. J. Neuroimmunol. 114, 207–212.

Miyagishi, R., Kikuchi, S., Fukazawa, T., Tashiro, K., 1995. Macrophage inflammatory protein-1 alpha in the cerebrospinal fluid of patients with multiple sclerosis and other inflammatory neurological diseases. J. Neurol. Sci. 129, 223–227.

Nagai, M., Usuku, K., Matsumoto, W., Kodama, D., Takenouchi, N., Moritoyo, T., Hashiguchi, S., Ichinose, M., Bangham, C.R., Izumo, S., Osame, M., 1998. Analysis of HTLV-I proviral load in 202 HAM/TSP patients and 243 asymptomatic HTLV-I carriers: high proviral load strongly predisposes to HAM/TSP. J. Neurovirol. 4, 586–593.

Osame, M., Usuku, K., Izumo, S., Ijichi, N., Amitani, H., Igata, A., Matsumoto, M., Tara, M., 1986. HTLV-I associated myelopathy, a new clinical entity. Lancet 1, 1031–1032.

Pala, P., Hussell, T., Openshaw, P.J., 2000. Flow cytometric measurement of intracellular cytokines. J. Immunol. Methods 243, 107–124.

Umehara, F., Izumo, S., Ronquillo, A.T., Matsumuro, K., Sato, E.,

Osame, M., 1994. Cytokine expression in the spinal cord lesions in HTLV-I-associated myelopathy. J. Neuropathol. Exp. Neurol. 53, 72–77.

Wu, X.M., Osoegawa, M., Yamasaki, K., Kawano, Y., Ochi, H., Horiuchi, I., Minohara, M., Ohyagi, Y., Yamada, T., Kira, J.I., 2000. Flow cytometric differentiation of Asian and Western types of multiple sclerosis, HTLV-I-associated myelopathy/tropical spastic paraparesis (HAM/TSP) and hyperIgEaemic myelitis by analyses of memory CD4 positive T cell subsets and NK subsets. J. Neurol. Sci. 177, 24–31.

Available online at www.sciencedirect.com
SCIENCE DIRECT
Microbes and Infection 6 (2004) 715–724
Microbes and Infection
www.elsevier.com/locate/micinf

Original article

Role of Nup98 in nuclear entry of human immunodeficiency virus type 1 cDNA

Hirotaka Ebina [a], Jun Aoki [a], Shunsuke Hatta [a], Takeshi Yoshida [a], Yoshio Koyanagi [b,*]

[a] *Department of Virology, Tohoku University Graduate School of Medicine, Sendai 980-8575, Japan*
[b] *Laboratory of Viral Pathogenesis, Institute for Virus Research, Kyoto University, 53 Shougoin-kawahara machi, Sakyou-ku, Kyoto 606-8507, Japan*

Received 18 February 2004; accepted 7 April 2004

Available online 24 May 2004

Abstract

Human immunodeficiency virus type 1 (HIV-1), like other lentiviruses, can infect non-dividing cells. The lentiviruses are most likely to have evolved a nuclear import strategy to import HIV-1 cDNA and viral protein complex through the nuclear pore complex (NPC) formed by nucleoporin proteins (Nup). In this study, we found that synthesis of integrated and 2LTR but not full-length form of HIV-1 cDNA was clearly impaired in culture via transduction of vesicular stomatitis virus matrix protein (VSV M), an inhibitor protein, through binding to the phenylalanine-glycine (FG) repeat region of Nup98. The impairment of synthesis of integrated and 2LTR DNA with VSV M was restored by ectopic overexpression of Nup98. A series of experiments using Nup98-depleted NPC by the small interfering RNA (siRNA) technique showed specific impairment of NPC structure and some functions, including nuclear import of HIV-1 cDNA. Our results suggest that Nup98 on the NPC specifically participates in the nuclear entry of HIV-1 cDNA following HIV-1 entry.
© 2004 Elsevier SAS. All rights reserved.

Keywords: Nucleoporin; NPC; HIV-1; Nuclear import

1. Introduction

The Retroviridae family of viruses can reverse transcribe their RNA genome into cDNA and then integrate the cDNA into host chromosomes. The lentiviruses (e.g. HIV) are distinguished by their ability to infect non-dividing cells, whereas the gamma-retroviruses (e.g. Moloney murine leukemia virus) require nuclear membrane dissolution to access the host cell DNA [1]. Thus, the lentiviruses are most likely to have evolved a nuclear import strategy, which allows their cDNA to cross the nuclear membrane independently of mitosis. In the case of human immunodeficiency virus type 1 (HIV-1), mitosis-independent replication was initially shown in terminally differentiated macrophages in vitro [1–3]. The mitosis-independent replication of HIV has also enabled the generation of integration-competent gene transfer vectors with promising therapeutic applications in a variety of non-dividing cellular hosts, including neurons [4], myocytes [5], and retinal cells [6]. To facilitate integration into a host DNA, a preintegration complex (PIC) is generated in the cytoplasm immediately after completion of reverse transcription. The PIC can be isolated successfully from in vitro freshly HIV-1-infected or HIV vector-infected cells and was recently shown to have the ability to traverse the nuclear pore complex (NPC) [1,7]. The NPCs serve as the conduits for bi-directional transport of macromolecules. Translocation across the NPC into the nucleus and from the nucleus into the cytoplasm is governed by a class of proteins known as importins and exportins (transport receptors), respectively. Both are members of the karyopherin family. The transport receptors engage the appropriate import or export signals and mediate their transport [8,9]. The PIC contains a double-strand linear cDNA as well as at least four viral proteins: matrix (MA), reverse transcriptase (RT), integrase (IN), and viral protein R (VPR), and has a diameter of approximately 56 nm, which greatly exceeds the 25 nm central channel of the NPC [1,7,10]. The NPC has a large supramolecular structure formed of ~50 unique proteins in eukaryotic cells, termed nucleoporins (Nup) [8,9,11,12]. High-resolution electron microscopic images of NPCs reveal an eightfold

* Corresponding author. Tel.: +81-75-751-4811; fax: +81-75-751-4812.
E-mail address: ykoyanag@virus.kyoto-u.ac.jp (Y. Koyanagi).

© 2004 Elsevier SAS. All rights reserved.
doi:10.1016/j.micinf.2004.04.002

symmetric structure, formed by nuclear and cytoplasmic rings and central spoke complex. The Nups often contain multiple phenylalanine-glycine (FG) dipeptide repeats clustered in domains, which in vertebrates are glycosylated by addition of *O*-linked *N*-acetylglucosamine (GlcNAc). Some of these Nups are localized asymmetrically at the NPC [9,11]. The asymmetric distribution of nucleoporins and the different affinities for import and export complexes may be important in determining the direction of transport [13,14]. Recent studies reported that importin 7 is involved in the nuclear entry of HIV-1 PIC as one of the main transport receptors [15]. However, the steps involved in the NPC remain largely undefined. In the present study, we show that nuclear import of HIV-1 cDNA requires NPC, and Nup98 has a role in nuclear entry of HIV-1 cDNA.

2. Materials and methods

2.1. Chemical treatment

Aphidicolin (APH) (Sigma Chemical Co., St. Louis, MO, USA), actinomycin D (ActD) (Sigma), zidovudine (AZT) (Sigma) or leptomycine B (LMB) (Sigma) was used. APH treatment (5 μg/ml) started 24 h before HIV-1 vector infection. AZT treatment started at the time of infection. LMB was added 2 h after infection. ActD was added 5 h after infection. DNA was extracted 24 h after infection.

2.2. Transfection

Human 293T cells were maintained in D-MEM containing 10% fetal calf serum (FCS). 293T cells were transfected with vesicular stomatitis virus matrix protein (VSV M)-, Nup98- or small interfering RNA (siRNA)-expressing DNA using calcium phosphate methods.

2.3. Quantitative polymerase chain reaction (PCR) assay

For the detection and quantification of individual forms of HIV-1 DNA, full-length/1LTR circle, 2LTR circle and integrated forms, we used a set of primer pairs and fluorogenic probes, as described previously [16,17]. PCR was performed using an ABI PRISM 7700 sequence detection system (PE-Applied Biosystems, Foster City, CA, USA) and TaqMan Universal PCR Master Mix (PE-Applied Biosystems). Cycling conditions included a hot start (50 °C for 2 min, 95 °C for 10 min), followed by 40 cycles of denaturation (95 °C for 15 s) and extension (60 °C for 1 min). To measure the integrated DNA, an *Alu*-sequence-specific sense primer and an antisense HIV-specific primer were used in the first PCR and subsequently 1000-fold diluted products were subjected to real-time PCR assay for measurement of R/U5 DNA, as described previously [16,17].

2.4. Cell-cycle analysis

Cell-cycle progression was examined by single-color flow cytometric analysis of the DNA content stained with 50 μg/ml of propidium iodine (Sigma).

2.5. DNA constructs and recombinant protein expression

Small interference RNA (siRNA)-expressing plasmid DNAs were constructed using the method described by Miyagishi and Taira [18]. The sequences inserted in the *Bfu*AI site of pU6i cassette, immediately downstream of the U6 promoter, were as follows: Nup98-targeted siRNA (siN98), 5′-CACC**GAATATGAAAG*T*AAGTT*A*TTA**TAGAATTACATCAAGGGAGAT**TAGTGACTTGCTTTCATATTC**TTTTTATGC-3′; firefly luciferase-targeted siRNA (siLuc), 5′-CACC**GTGCG*T*TG*T*TGGTG*TT*AA*T*CC**ATCTCCCTTGATGTAATTCTA**GGGTTGGCACCAGCAGCGCAC**TTTTTATGC-3′. Bold-lettered nucleotides are the siRNA sequences, italic nucleotides are mutated, and underlined nucleotides are loop sequences. The siRNA-expressing DNA fragment was also inserted into the *Eco*RI site of a lentivirus vector DNA, pCS-CDF-EH2K^k, and an enhanced green fluorescence protein (EGFP) fragment between the *Age*I and *Xho*I sites of pCS-CDF-EG-PRE [19] was replaced with a H-2K^k fragment (Daiichi pure chemicals, Tokyo, Japan).

HA-tagged human Nup98-expressing plasmid DNA (p37R-HANup98) and EGFP-fused VSV M-expressing DNA (pEGFPN3-M) [20] were kindly provided by Dr. Elisa Izaurralde (European Molecular Biology Laboratory). A *Bss*HII-*Xho*I DNA fragment covering the coding region of HA-tagged human Nup98 region was cloned into a site downstream of CMV promoter in pcDNA3.1/Zeo (+) (Invitrogen, Carlsbad, CA, USA) (pcDNup98). Alanine substitutions from Asp-Thr-Tyr at the position of VSV M 52–54 [VSV (M)] were introduced using an oligonucleotide-directed in vitro mutagenesis system (Quickchange site-directed mutagenesis, Stratagene, San Diego, CA, USA). DsRed-fusion recombinant protein with NLS, U1A and rpL23a was produced in *Escherichia coli*. A double-strand synthetic nucleotide of SV40 NLS (5′-CCA TGC ATA TGC CAA AAA AGA AGA GAA AGG TTG-3′) and PCR-amplified DNA fragment of U1A (1–486), or rpL23a (1–486) from mRNA of HeLa cells was cloned into the *Sma*I or *Sal*I-*Bam*HI sites of pDsRed1-N1 (Clontech, Palo Alto, CA, USA), and then a *Sal*I-*Not*I fragment was inserted in the *Sal*I-*Not*I site of pGEX-4T-2 (Amersham Pharmacia Biotech, Piscataway, NJ, USA). *E. coli* ER2566 (New England Biolabs Inc., Beverly, MA, USA) was used, and recombinant proteins were purified on glutathione sepharose 4 Fast Flow (Amersham) by standard protocols, as previously described [21].

2.6. Reverse-transcription PCR

Total RNA was extracted from transiently transfected cells by using a RNeasy RNA-preparation Kit (Qiagen, KJ

Venlo, The Netherlands). Reverse transcription and PCR were carried out using a SuperScript One-Step RT-PCR with Platinum Taq (Invitrogen). We used the following primers to detect the specific transcripts: for Nup107, 5′-AAACGCGGTAGCTAAACTGCA-3′, 5′-ACCACCAGCTGACTTTGTCGA-3′; for Nup214, 5′-CTTGCCACGAAAACCGTGA-3′, 5′-CAACCCGCAGTCCTGAAAA-3′; for p62, 5′-CAGACACCGACGGATTTGCTT-3′, 5′-TGGATGTTGTTGTGGAGGTGC-3′; for Nup98, 5′-TCTCATCCCAAAACAATGCCTT-3′, 5′-AAACAAAGATGCCTGTCCAGCA-3′; for Nup153, 5′-TGACAATGAAGAGCCAAAGTGT-3′, 5′-TAGGAGTTGTTCCAGAGCCAAA-3′. TaqMan GAPDH Control Reagents (PE-Applied Biosystems) were used as primer sets for glyceraldehyde 3-phosphate dehydrogenase (GAPDH). Fifty nanograms of template RNA and 10 pmol of specific primers were used. The efficiency of PCR amplification was roughly in the linear range, as determined by preliminary test with increasing number of cycles. Finally, the PCR products were analyzed by agarose gel electrophoresis using standard techniques.

2.7. Virus vector infection

For HIV-1 vector preparation, a replication-incompetent EGFP-expressing lentivirus (pCS-CDF-CG-PRE) or siRNA-expressing lentivirus was co-transfected into 293T cells along with VSV G-expressing plasmid (pVSV G), HIV-Gag-Pol-expressing plasmid (pRRE) and Rev-expressing plasmid (pRSV-Rev) as described before [6,19]. Three days after transfection, the culture supernatants were cleared by filtration and concentrated through centrifugation at 6000 × *g* for 16 h at 4 °C. The transducing unit (TU) was determined by measurement of EGFP-, or H-2K^k-expressing cells using flow cytometry. Phycoerythrin-labeled anti-mouse H-2K^k monoclonal antibody (mAb) (Cedarlane, Ontario, Canada) was used. Cells were analyzed on FACS SCAN, using Cell Quest software (BD PharMingen, San Diego, CA, USA). Treatment with DNaseI (20 μg/ml) was performed to remove plasmid DNA in the virus stocks. Heat-inactivated (65 °C, 30 min) virus liquid was used as negative control for HIV DNA quantification in infected cells. APH-treated MT-2 cells or 293T cells (2×10^5 cells) were infected with HIV-1 vector (4×10^5 TU). Two hundred thousand 293T cells were transfected with VSV M- or Nup98-expressing DNA and then 24 h later, infected with HIV-1 vector (4×10^5 TU). Two hundred thousand 293T cells were transfected with siRNA-expressing DNA and then 72 h later, infected with HIV-1 vector (4×10^5 TU). The amount of viral DNA was measured by the quantitative PCR assay 24 h after infection, as described above. HeLa cells (1×10^5 cells), grown on cover-slips, were infected with siRNA-expressing HIV-1 vector at multiplicity of infection (m.o.i.) of 1. The cells were analyzed 96 h later by immunofluorescence, immunoblotting or nuclear import assay.

2.8. Immunofluorescence analysis

HeLa cells, grown on cover-slips, were washed twice with phosphate-buffered solution (PBS) and fixed in 4% (vol/vol) paraformaldehyde/PBS for 15 min at room temperature. The cells were permeabilized with 0.2% Triton X-100/PBS for 5 min. After blocking with 5% bovine serum albumin (BSA)/0.1% Triton X/PBS for 1 h, the cells were incubated with an NPC-specific mouse mAb, mAb414 (BabCO, Berkeley, CA, USA) or anti-Nup98 polyclonal antibody (C-16) (Santa Cruz Biotechnology Inc., Santa Cruz, CA, USA) at 4 °C overnight. Cells were washed three times with 0.05% Triton X/PBS and then incubated with Alexa 594-conjugated goat anti-mouse IgG antibody (Molecular Probes, Eugene, OR, USA) or fluorescein isothiocyanate (FITC)-conjugated donkey anti-goat IgG antibodies (Chemicon, Temecula, CA, USA) for 1 h. Cells were washed three times with 0.05% Triton X/PBS, mounted in Vectashield mounting medium for fluorescence (Vector Laboratories, Burlingame, CA, USA) and analyzed with a Leica QFluoro system. The cells were also stained with Hoechst 33342 (Molecular Probes).

2.9. Nuclear import assay

HeLa cells grown on cover-slips were washed in PBS and permeabilized for 5 min on ice in 50 μg/ml digitonin (Sigma)/transport buffer (20 mM Hepes– NaOH, pH 7.3, 110 mM CH_3COOK, 2 mM $(CH_3COO)_2Mg$, 5 mM CH_3COONa, and 2 mM dithiothreitol). After washing three times with transport buffer, cells were incubated at 30 °C for 30 min in the presence of energy-regenerating system (1 mM ATP, 1 mM GTP, 10 mM creatine phosphate, and 20 U/ml creatine phosphokinase), 3 μM DsRed-labeled recombinant protein, and cytoplasmic extract from 2×10^5 HeLa cells. Samples were washed three times in transport buffer, fixed on ice for 30 min with 1% formalin/transport buffer and analyzed with a Leica QFluoro system.

2.10. Immunoblotting

293T cells were co-transfected with an HA-tagged human Nup98-expressing plasmid DNA (pcDNup98) and a siRNA-expressing plasmid (siN98 or siLuc). Three days after transfection, the cells were washed twice and lysed in RIPA buffer (0.5% NP-40 in 20 mM Tris–HCl [pH 8.2], 0.15 M NaCl, 5 mM iodoacetamide, and 1 mM phenylmethylsulfonyl fluoride). After loading on SDS/PAGE, polypeptides were transferred to Immobilion Transfer Membranes (Millipore, Billerica, MA, USA), the level of Nup98 was determined using a goat anti-Nup98 polyclonal antibody (C-16), biotin-conjugated rabbit anti-goat IgG (Chemicon) and then incubated with horseradish peroxidase (HRP)-conjugated streptavidin (Zymed, San Francisco, CA, USA). The filter generated from HeLa cells infected with siRNA-expressing

HIV-1 vector as described above was also incubated with mAb414 (mainly reactive against p62), biotin-conjugated horse anti-mouse IgG (VECTOR) and HRP-conjugated streptavidin. The specific bands were detected using Western Lighting Chemiluminescence Reagent (Perkin–Elmer Life Science, Boston, MA, USA). For detection of Nup98-VSV M complex, 293T cells were co-transfected with Nup98-expressing plasmids (pcDNup98) and EGFP-fused VSV M-expressing plasmid DNA (pEGFPN3-M) or the mutant [VSV M(D)]. Two days after transfection, the cells were lysed in triple detergent lysis buffer (1% NP-40, 0.1% SDS, 0.5% sodium deoxycholate in 50 mM Tris–HCl [pH 8.0], 0.15 M NaCl, 1 μg/ml aprotinin, 1 mM phenylmethylsulfonyl fluoride), and a mouse anti-HA mAb (F-7) (Santa Cruz) was added. After incubation for 12 h at 4 °C with protein G-sepharose (Amersham), the precipitate was washed three times with triple detergent lysis buffer, and the bound proteins were eluted by 1× sample buffer (1.71% SDS in 175 mM Tris–HCl [pH 6.8], 5% glycerol, 1% 2-mercaptoethanol) at 37 °C for 30 min. The samples were loaded on SDS/PAGE and transferred to Immobilon Transfer Membranes. For detection of the Nup98, a goat anti-Nup98 polyclonal antibody (C-16) (Santa Cruz) and biotin-conjugated rabbit anti-goat IgG (Chemicon) were used. For detection of VSV M, a rabbit anti-GFP polyclonal antibody (Santa Cruz) and biotin-conjugated donkey anti-rabbit IgG (Chemicon) were used.

2.11. Statistical analysis

All data were expressed as mean ± standard deviations (S.D.). Differences between groups were examined for statistical significance using the Welch's *t*-test. A P value less than 0.05 denoted the presence of a statistically significant difference.

3. Results

3.1. Efficient nuclear import of HIV-1 cDNA in infected cells

It has been shown that HIV and HIV-based lentivirus vectors efficiently infect non-dividing cells [2,6]. To determine the integration efficiency in dividing and non-dividing cells, we prepared cell-cycle-arrested T cell culture using MT-2 cells treated with APH, an inhibitor of DNA polymerase α. Under this condition, cell-cycle was confirmed to be stopped at G1 phase from flow cytometric analysis (Fig. 1A). The same numbers of treated (arrested) or untreated (proliferating) cells were infected with the same amounts of HIV-1 vector and the arrested culture was further maintained in the presence of APH. Since in this experiment we used a single-round infection system, we could estimate the precise efficiency of reverse transcription, nuclear translocation as well as integration. Total DNA was extracted 24 h after infection and a set of real-time PCR assay was performed [16,17]. Using this assay, we were able to measure the full-length/1LTR circle, 2LTR circle and integrated forms of HIV-1 cDNA, respectively. Since the 2LTR circle and integrated forms are found only in nucleus after HIV infection [3,22], we could estimate the efficiency of nuclear entry as well as integration of HIV-1 cDNA. Fig. 1B shows that the levels of integrated, 2LTR and full-length/1LTR circle form in proliferating cultures were higher than those in arrested cultures, because the numbers of the cells were two to three times greater in proliferating culture. However, significant amounts of integrated ($4.2 \times 10^5 \pm 5.4 \times 10^4$ copies per culture) and 2LTR ($1.5 \times 10^5 \pm 1.5 \times 10^3$ copies per culture) form DNA were found in the arrested culture (Fig. 1B). Similar results were also obtained in APH-treated 293T cells (data not shown). These data correspond well with the previously reported findings of the high susceptibility of APH-treated cells to HIV-1 [3,22]. Importantly, the ratios of integrated form and 2LTR form to full-length/1LTR form were similar in the proliferating (integrated; 0.108 ± 0.024, 2LTR; 0.022 ± 0.002, full-length/1LTR; 1.0) and the arrested cultures (integrated; 0.09 ± 0.011, 2LTR; 0.031 ± 0.001, full-length/1LTR; 1.0), respectively, strongly suggesting that HIV-1 cDNA efficiently traverse NPC, depending on the active nuclear import machinery in not only non-dividing cells but also proliferating cells.

3.2. Inhibition of HIV-1 cDNA import with a Nup98-specific inhibitor

Next, to examine the specificity of our real-time PCR assay and the associated molecules in nuclear entry of HIV-1 cDNA, we prepared HIV reverse transcription-inhibited (AZT-treated), transcription-blocked (ActD-treated), or CRM1-dependent nuclear export-inhibited (LMB-treated) 293T cell cultures. As expected, AZT significantly inhibited the appearance of all forms of DNA (Fig. 2A a–c). Although dose-dependent inhibition of integration was found in ActD- or LMB-treated cultures, significant accumulation of the 2LTR form was also found (Fig. 2A f and i), suggesting that newly synthesized proteins as well as CRM1-dependent exported proteins may be required for the efficient integration but not nuclear entry of HIV-1 cDNA. To examine whether specific Nups are required for HIV infection, we used VSV M protein, a specific inhibitor protein against Nup98. It has been shown that Nup98 is involved in the nuclear import of some proteins as well as the export of RNA, and its function is specifically impaired in the presence of VSV M protein [20]. The VSV M binds a region within residues 66–515 of Nup98 that encompasses most of the FG repeats, the hRAE1/Gle2 binding site or GLEBS-like motif [23], and most of the predicted glycosylation sites of the Nups. Through these sites, Nup98 was able to interact with three